

Unveiling the CO₂ Adsorption Capabilities of Biphenylene Network Monolayers through DFT Calculations

K. A. Lopes Lima^a, L. A. Ribeiro Junior^{a,b,*}

^aUniversity of Brasília, Institute of Physics, 70.910-900, Brasília, Brazil.

^bComputational Materials Laboratory, LCCMat, Institute of Physics, University of Brasília, 70910-900, Brasília, Brazil

ARTICLE INFO

Keywords:

Biphenylene Network
Oxygen Molecule
Vacancy
Adsorption
Density Functional Theory.

ABSTRACT


Nanomaterial synthesis and characterization advancements have led to the discovery of new carbon allotropes, such as the biphenylene network (BPN). BPN consists of four-, six-, and eight-membered rings of sp²-hybridized carbon atoms. Here, we employ density functional theory (DFT) calculations to investigate the CO₂ adsorption capabilities in pristine and vacancy-endowed BPN monolayers. Our findings indicate that BPN lattices with a single-atom vacancy exhibit higher CO₂ adsorption energies than pristine BPN. Unlike other 2D carbon allotropes, BPN does not exhibit precise CO₂ sensing and selectivity by altering its band structure configuration. In pristine lattices, CO₂ molecules are physisorbed in the eight-membered rings, while defective regions of vacancy-endowed lattices enable chemisorption of CO₂. Regarding CO₂ physisorption, the recovery time values are minimal, suggesting a rapid interaction between BPN and this molecule, with negligible relaxation time required to alter the electronic properties of BPN lattices.

1. Introduction

Two-dimensional (2D) carbon allotropes have garnered considerable attention due to their unique properties and wide-ranging applications across various fields [1, 2]. Comprised solely of carbon atoms, they typically possess an ultra-thin thickness of just one atom, leading to distinct properties that set them apart from their 1D and 3D counterparts [3]. 2D carbon allotropes exhibit exceptional structural characteristics, offering versatility and customization for applications in flat electronics [4, 5]. Moreover, their atomic-level structural modifications enable precise tailoring of their properties to meet specific application requirements [6].

Graphene, a single layer of carbon atoms arranged in a hexagonal lattice, is one of the most renowned 2D carbon allotropes [7]. Its excellent electrical conductivity [8], impressive mechanical strength [9], and thermal stability [10] position it as a promising material for a diverse range of applications in electronics [11], energy storage [12], and other fields [13, 14]. However, the absence of a band gap in graphene poses a hurdle for specific electronic applications like transistors or digital logic circuits, which necessitate materials with semiconducting band gaps [15, 16]. Consequently, researchers have explored various approaches to introduce a band gap into graphene [17] or develop novel materials that retain its unique properties while possessing a well-defined band gap [18–20].

Recently, various novel 2D carbon allotropes have emerged, significantly expanding the pool of available materials for potential applications [18–24]. These include monolayer amorphous carbon [23], monolayer fullerene network

 ribeirojr@unb.br (L.A.R. Junior)
ORCID(s):

[19, 20], gamma-graphyne [18, 24], and the biphenylene network (BPN) [19]. Of particular interest is the BPN, an sp²-hybridized carbon allotrope boasting a flat structure with a well-organized arrangement of four-, six-, and eight-membered rings of carbon atoms [19]. Its synthesis involved an on-surface interpolymer dehydrofluorination reaction, resulting in an exceptionally flat structure. Notably, the BPN exhibits metallic behavior, rendering it suitable for applications such as a conducting wire or anode material in lithium-ion batteries, offering promising prospects for its usage [25–28].

BPN offers a fresh perspective for exploring non-graphene sp² carbon allotropes and their distinctive characteristics. Notably, BPN possesses eight-membered rings that form pores capable of efficiently trapping and adsorbing small molecules like CO₂ and methane [29, 30]. This attribute positions BPN as a promising contender for devising strategies to mitigate the adverse impacts of increasing atmospheric CO₂ levels. Although many nanostructured materials have been explored for their CO₂ adsorption capabilities [31–33], studies in the literature have yet to investigate the potential of BPN for CO₂ adsorption.

In this study, we employed density functional theory (DFT) calculations to investigate the adsorption capability of both pristine and vacancy-endowed BPN monolayers regarding CO₂. BPN lattices with a single-atom vacancy exhibit higher CO₂ adsorption energies than pristine counterparts. Unlike graphene and other 2D carbon allotropes, BPN lattices do not rely on changes in their band structure configurations for precise CO₂ sensing and selectivity.

2. Methodology

Our study aimed to investigate the impact of CO₂ adsorption on the electronic and structural properties of pristine and vacancy-endowed BPN lattices through DFT calculations. We used the DMol3 code [34, 35] within the Biovia Materials Studio software [36] to perform these calculations. For a proper treatment of van der Waals interactions, we employed the Grimme scheme [37] and employed the Perdew-Burle-Ernzerhof (PBE) functional [37–39] with unrestricted spin (DNP) within the framework of the exchange-correlation generalized gradient approximation (GGA). We incorporated semi-core DFT pseudopotentials to accurately describe the interactions between valence electrons and atomic nuclei and employed a numerical basis set of atomic orbitals with polarized functions. Additionally, we accounted for the basis set superposition error (BSSE) correction [40] using the counterpoise method to ensure the precision and reliability of our results.

To optimize the system's geometry, we implemented several parameters to ensure the accuracy of our calculations. A $5 \times 5 \times 2$ Monkhorst-Park k-point mesh in the Brillouin zone [41] was used. Additionally, we set a self-consistent field (SCF) tolerance of 1×10^{-5} eV/atom and established a maximum force on each atom of $0.001 \text{ Ha}/\text{\AA}$. A maximum value of 0.005 \AA was adopted for the atomic displacement. We employed a vacuum spacing of 30 \AA in lattices with dimensions of $2 \times 2 \times 1$ to prevent interactions between layer images. Moreover, cutoff energy of 450 eV and a $10 \times 10 \times 2$

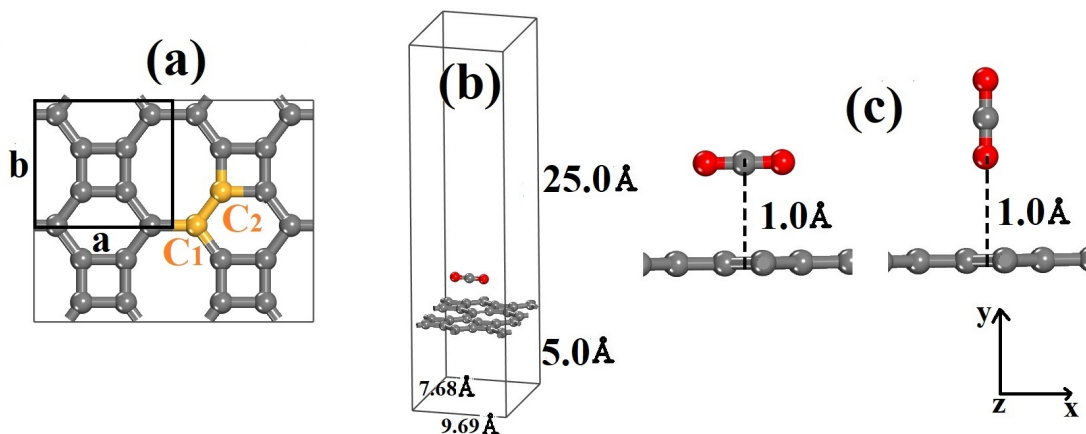


Figure 1: In panel (a), a schematic representation of the optimized pristine BPN sheet is presented, which includes the unit cell with lattice vectors a and b . In yellow, the atoms C_1 and C_2 represent the lattice sites where vacancies are imposed. The initial configuration for the BPN/CO₂ system is presented in panel (b). Panel (c) shows the side view of the BPN/CO₂ system, highlighting the initial distance between CO₂ (in its horizontal and vertical alignments) and the BPN sheet. Oxygen and carbon atoms are red and grey, respectively.

Monkhorst-Park k-point were employed. It is important to note that these parameters have previously proven successful in studying small molecule adsorption on nanostructured surfaces [42–46].

Figure 1(a) illustrates the unit cell of the optimized BPN monolayer featuring lattice vectors a and b . The BPN structure consists of a unit cell with 6 atoms and belongs to the $P1$ plane group, with lattice parameters measuring 4.26 Å and 3.88 Å, which aligns with previous findings [47–49]. The initial configuration of the BPN/CO₂ systems is presented in Figure 1(b). For clarity, Figure 1(c) provides a side view of the initial configurations, highlighting the initial distance of 1.0 Å between CO₂ and the BPN sheet, with CO₂ positioned in both horizontal and vertical alignments.

3. Results

We initiate our discussion by presenting the optimized configurations for all the BPN@CO₂ systems examined in this study, following the representation in Figures 1(b-c). The outcomes for the pristine case (BPN@CO₂), C_1 vacancy case (BPN-DEF/ C_1 @CO₂), and C_2 vacancy case (BPN-DEF/ C_2 @CO₂) with the initial orientations of the CO₂ molecule in both the vertical (V) and horizontal (H) directions are exhibited in Figures ??(a)-(f). DEF denotes defective lattices.

The initial position of the CO₂ molecule underwent displacement in all the examined cases, resulting in adsorption distances of 3.18 Å, 3.10 Å, 2.95 Å, 3.14 Å, 0.52 Å, and 0.49 Å for BPN@CO₂-V, BPN-DEF/ C_1 @CO₂-V, BPN-DEF/ C_2 @CO₂-V, BPN@CO₂-H, BPN-DEF/ C_1 @CO₂-H, and BPN-DEF/ C_2 @CO₂-H, respectively. Among all the

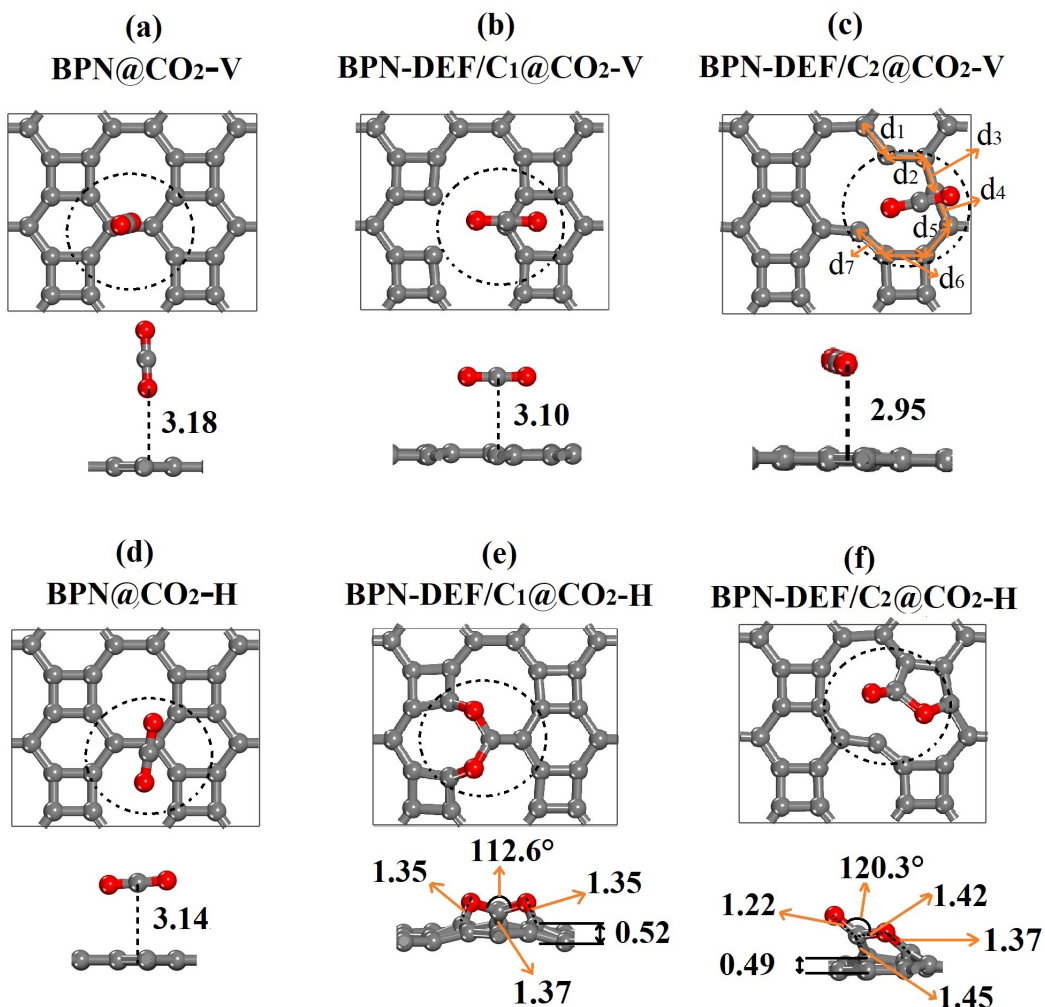


Figure 2: (a-f) show schematic representations of the optimized configurations for the BPN/CO₂ cases: (a-f) BPN@CO₂-V, BPN-DEF/C₁@CO₂-V, BPN-DEF/C₂@CO₂-V, BPN@CO₂-H, BPN-DEF/C₁@CO₂-H, BPN-DEF/C₂@CO₂-H, respectively. Oxygen and carbon atoms are red and grey, respectively. In panel (c), the orange arrows stand for the novel C-C bonds (d₁, d₂, d₃, d₄, d₅, d₆, and d₇) formed after bond reconfiguration imposed by the vacancy type C₂. DEF denotes defective lattices.

cases examined, only the pristine case (BPN@CO₂-V, Figure 2(a)) demonstrated a minimal change in the initial orientation of the vertically positioned molecule following structure optimization. In the cases shown in Figures 2(b-d), the CO₂ molecule maintained its horizontal alignment relative to the BPN sheet throughout the optimization process. These interactions between BPN and CO₂ in Figures 2(a-d) are characterized by a physisorption mechanism during adsorption.

Conversely, Figures 2(e) and 2(f) demonstrate that BPN and CO₂ interact through a chemisorption mechanism. This adsorption type disrupts the BPN lattice locally, forming a localized buckling with a magnitude of approximately 0.5 Å. In Figure 2(e), all CO₂ atoms establish bonds with BPN atoms within a range of 1.35-1.37 Å, inducing a new angle in the CO₂ molecule of 112.6°. In Figure 2(f), only two atoms from the CO₂ molecule bind to the BPN, forming bonds with lengths ranging from 1.37-1.45 Å. In this case, the molecule's resulting angle is 120.3°.

In the BPN@CO₂-V and BPN@CO₂-H cases (Figures 2(a) and 2(d), respectively), the CO₂ molecule was adsorbed in proximity to two adjacent octagonal rings, indicating an adsorption mechanism in pristine BPN that is independent of molecule orientation. On the other hand, in the defective cases BPN-DEF/C₁@CO₂-V and BPN-DEF/C₂@CO₂-V (Figures 2(b) and 2(c), respectively), CO₂ was adsorbed peripherally to the defect, resulting in similar adsorption distances.

In contrast to previous DFT studies on CO₂ adsorption on graphene [50], defects in BPN have minimal impact on the adsorption distance or CO₂ orientation. This feature can be attributed to the presence of the eight-atom ring in the BPN structure, which acts as a pore and exhibits a slightly weaker interaction potential than a single-atom vacancy in the lattice. In the case of graphene, for example, a twelve-atom ring resulting from a single-atom vacancy forms a larger pore diameter than the other hexagonal rings in its structure [50]. For the C₂ vacancy cases, the pore region undergoes bond reconfiguration (see Figures 2(c) and 2(f)). The new C-C bonds, indicated by the orange arrows in Figure 2(c), are $d_1 = 1.42$, $d_2 = 1.45$, $d_3 = 1.40$, $d_4 = 1.39$, $d_5 = 1.48$, $d_6 = 1.52$, and $d_7 = 1.37$.

To comprehensively analyze the adsorption energies of the BPN/CO₂ complexes, we have generated adsorption energy maps for all cases, as shown in Figure 3. These maps were created by systematically varying the position of the CO₂ molecule along the x and y directions of the BPN surface, with a step size of 0.5 Å. The CO₂ molecule was positioned 3.0 Å above the BPN surface in these calculations. A clear trend emerges, with the regions inside the octagonal rings displaying lower adsorption energies, ranging from -0.22 eV to -0.08 eV. Furthermore, Figure 3 emphasizes that interaction energies are significantly lower in regions with lattice defects and where the CO₂ molecule is aligned horizontally, ranging from -0.22 eV to -0.27 eV.

In the BPN@CO₂-V case (Figure 3(a)), the center of the octagonal rings exhibits the lowest adsorption energies, indicating stronger interaction between BPN and an oxygen atom in the CO₂ molecule. In the BPN@CO₂-H case (Figure 3(d)), the regions with the lowest adsorption energies extend towards the C-C bonds due to the proximity of the carbon atom in the molecule to the BPN plane. In these cases, the adsorption energies for CO₂ range from -0.11 eV to -0.06 eV.

The BPN lattice with a C₁ vacancy type shows the largest pore region among all the structures studied, as depicted in Figures 3(b) and 3(e). The CO₂ adsorption energies for the BPN-DEF/C₁@CO₂-V and BPN-DEF/C₁@CO₂-H cases range from -0.22 eV to -0.08 eV. In the DEF/C₂@CO₂-V case, the adsorption energies vary from -0.16 eV to

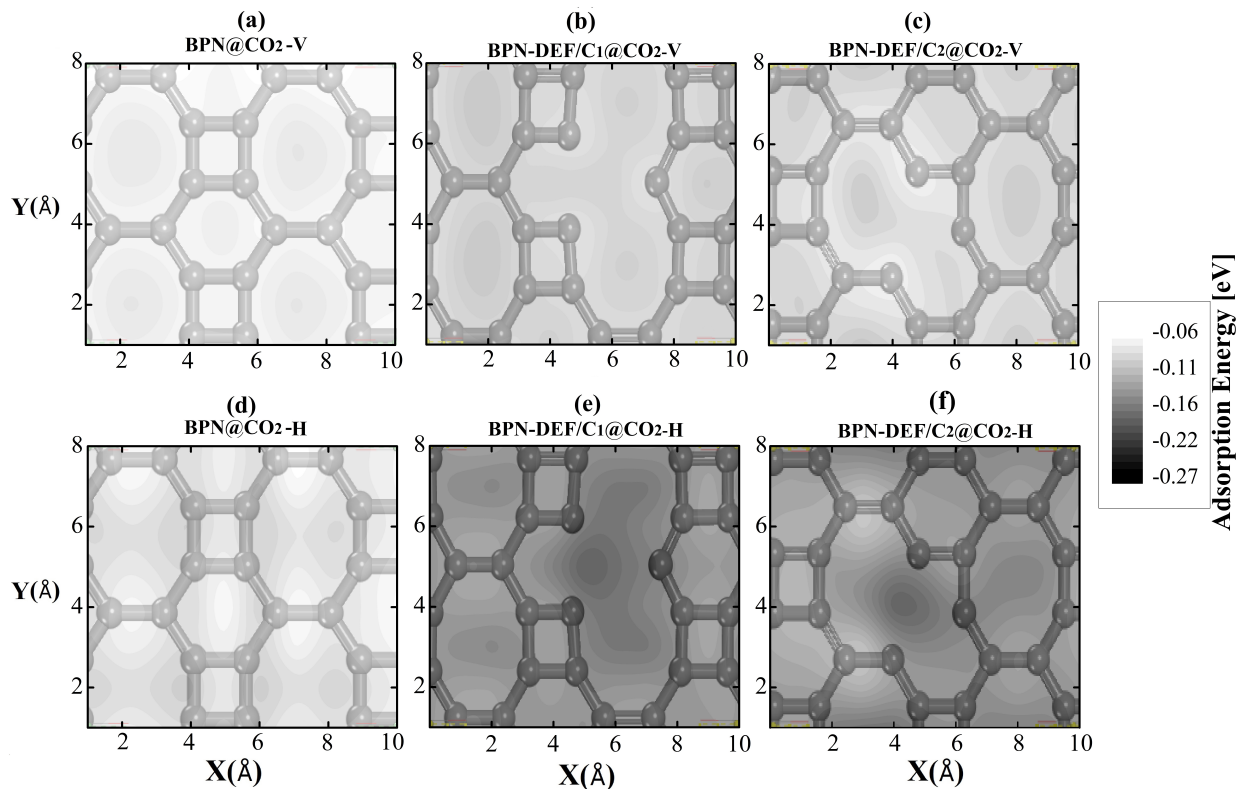


Figure 3: Adsorption energy maps for the minimum energy configurations in the (a) BPN@CO₂-V, BPN-DEF/C₁@CO₂-V, (b) BPN-DEF/C₂@CO₂-V, (c) BPN@CO₂-H, (d) BPN-DEF/C₁@CO₂-H, and (f) BPN-DEF/C₂@CO₂-H cases.

-0.08 eV. The lowest CO₂ adsorption energy (-0.25 eV) is observed in the BPN-DEF/C₂@CO₂-H case, as shown in Figure 3(f).

To visualize the localization of the Highest Occupied Molecular Orbital (HOMO, in green) and Lowest Unoccupied Molecular Orbital (LUMO, in red), we present Figure 4. Importantly, the HOMO and LUMO orbitals provide valuable insights into the electronic structure of the nanostructure and the adsorbed molecule. By visualizing these orbitals, we can determine the distribution and localization of electronic states, identify bonding and antibonding regions, and assess the interaction between the molecule and the nanostructure. Generally, the HOMO and LUMO orbitals span across the BPN lattice. In the pristine case, they are localized on the C-C bonds forming the square ring, as depicted in Figures 4(a) and 4(d).

With the presence of a single-atom vacancy, the well-ordered distribution pattern of the HOMO and LUMO orbitals observed in the pristine case is disrupted, and these orbitals are scattered randomly around the vacancy region, as shown in Figures 4(b,c,f). Interestingly, for the case BPN-DEF/C₁@CO₂-H (see Figure ??(e)), the binding of the CO₂ molecule to the BPN lattice leads to reforming the previously defective octagon. In this process, the distribution of

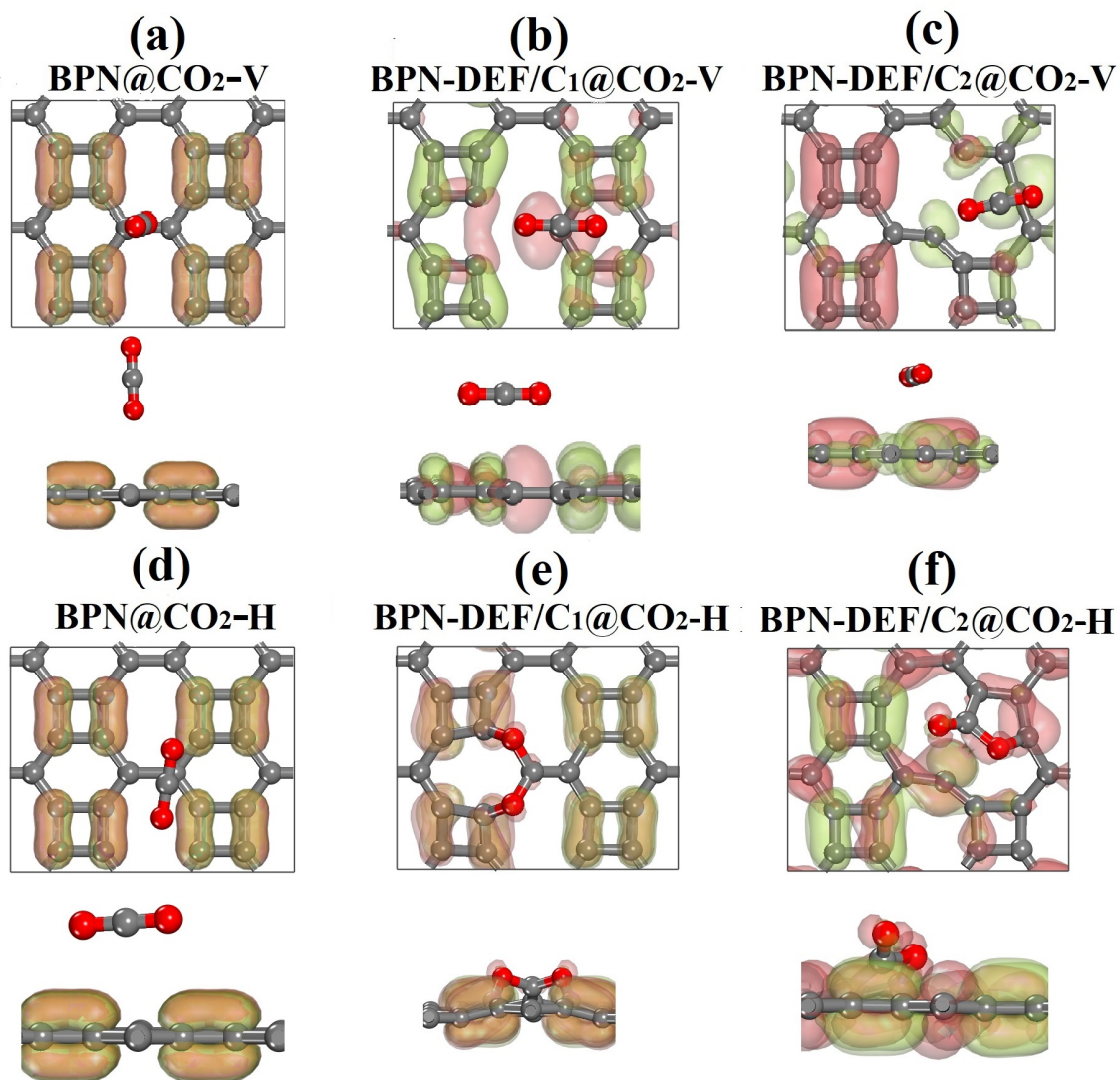


Figure 4: Schematic representation for the distribution of the Highest Occupied Molecular Orbital (HOMO, in green) and Lowest Unoccupied Molecular Orbital (LUMO, in red) configurations.

the HOMO and LUMO orbitals undergoes a transition, resembling the configuration observed in the pristine case. In chemisorption cases (see Figures 4(e) and 4(f)), a portion of the LUMO orbital is found on the CO₂ molecule. This process results in a slight charge transfer from BPN to CO₂, as indicated in Table 1.

Next, we focus on the recovery time (τ), representing the duration required for stabilizing adsorption. A higher τ value indicates better adsorption performance. We calculate τ using the equation $\tau = \nu^{-1} \times \exp(-E_{\text{ads}}/k_B T)$, where ν corresponds to the oscillation frequency of the molecule (10^{12} s^{-1} [51]), k_B is the Boltzmann constant, and T denotes the temperature (298 K).

Upon examining Table 1, we observe that both τ and the transferred charge (Q_t) increase with the adsorption energy

Table 1

Calculated adsorption energies (E_{ads}), amount of transferred charge from CO₂ to BPN (Q_t), and the recovery time τ (s).

Structures	E_{ads} (eV)	Q_t (e)	τ (s)
BPN	---	---	---
BPN@CO ₂ -V	-0.22	-0.001	5.25×10^{-9}
BPN@CO ₂ -H	-0.31	-0.001	1.74×10^{-7}
BPN-DEF/C ₂ @CO ₂ -V	-0.54	-0.003	1.35×10^{-3}
BPN-DEF/C ₁ @CO ₂ -V	-0.65	-0.005	9.80×10^{-2}
BPN-DEF/C ₁ @CO ₂ -H	-3.52	-0.47	---
BPN-DEF/C ₂ @CO ₂ -H	-3.60	-0.25	---

(E_{ads}). Table 1 summarizes the E_{ads} , Q_t , and τ values obtained for each case. The system with the longest recovery time is BPN-DEF/C₁@CO₂-V, approximately 9.80×10^{-2} s. Conversely, the pristine case BPN@CO₂-V exhibits the shortest recovery time, around 5.25×10^{-9} s. These relatively small τ values suggest that the interaction between BPN and CO₂ occurs rapidly, without a significant relaxation time required to alter the BPN electronic band structure, as discussed below.

Finally, Figure 5 showcases the electronic band structure for all the cases discussed here. The dashed red line denotes the Fermi level. Previous studies on the electronic band structure of pristine BPN can be found in references [47–49]. Pristine BPN displays a metallic signature with a Dirac cone in the middle of the band along the G-K and X-M paths. The band structure configurations for isolated pristine BPN and vacancy-endows BPN lattices are presented in the Supplementary Material.

The presence of a single-atom vacancy disrupts this band profile, resulting in the elimination of the Dirac cones and the opening of a small bandgap of approximately 100 meV. Interestingly, BPN does not exhibit precise CO₂ sensing and selectivity by altering its band structure configuration. The adsorption of CO₂ does not significantly alter the band dispersion profiles of the BPN lattices, as evidenced by their low energy adsorption and quick recovery times. Unlike other 2D carbon allotropes [32, 33, 50?], BPN lattices do not exhibit precise CO₂ sensing and selectivity based on changes in their band structure configurations.

4. Conclusions

Our study employed DFT calculations to analyze the CO₂ adsorption characteristics of pristine and vacancy-endowed BPN monolayers. The computational approach involved generating potential energy maps to identify specific regions of the BPN surface with lower CO₂ adsorption energies.

The obtained adsorption distances and energy values collectively suggest CO₂ adsorption through physisorption and chemisorption mechanisms. In the pristine BPN cases, we observed that the CO₂ molecule was adsorbed near two octagonal rings, implying an adsorption mechanism independent of the molecule's orientation. Conversely, in the

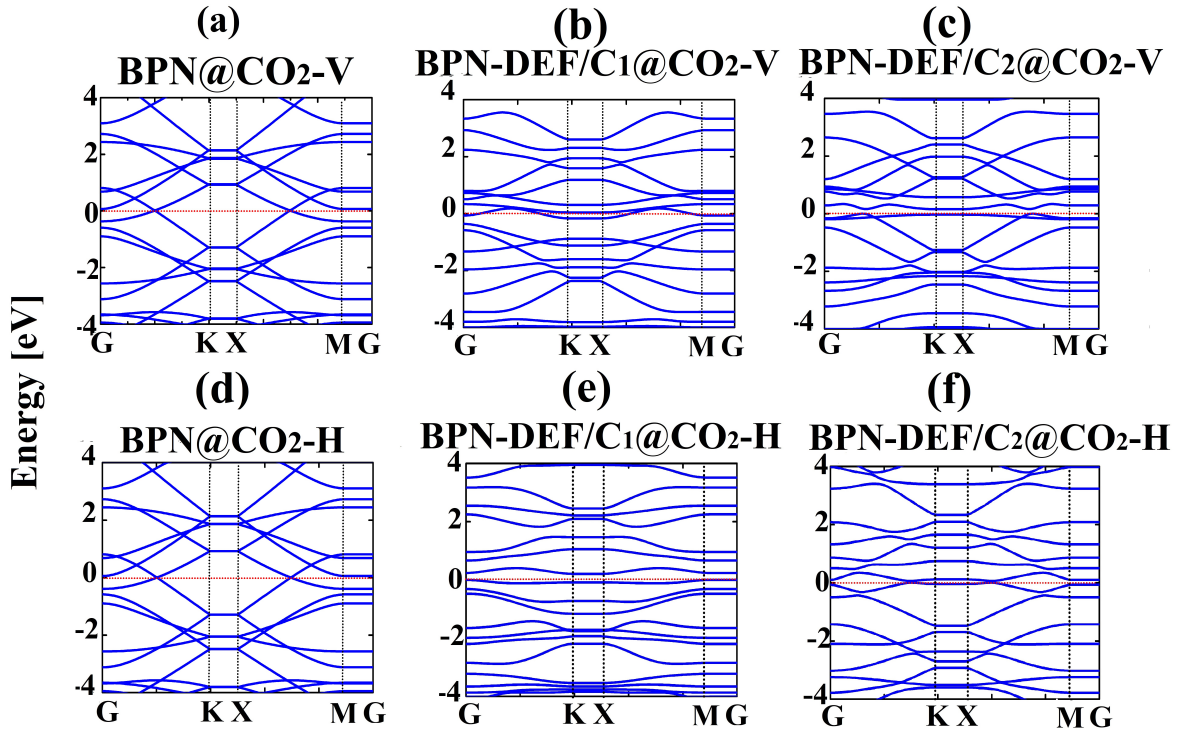


Figure 5: The electronic band structures for all the cases studied here. The dashed red line represents the Fermi level.

defective cases with vertically aligned CO₂, this molecule was adsorbed peripherally to the defect, resulting in similar adsorption distances.

Defects in BPN have a negligible impact on the adsorption distance, but they are sensitive to the CO₂ orientation. This distinction can be attributed to an eight-atom ring within the BPN structure, which functions as a pore with a slightly weaker interaction potential than a single-atom vacancy in the lattice. The physisorption process prevailed when the CO₂ molecule was aligned vertically concerning the BPN surface. However, when the CO₂ molecule was aligned horizontally on the BPN surface, the adsorption process was dominated by chemisorption.

A clear trend emerged in analyzing the adsorption maps. The adsorption energies tend to present suitable values in regions inside the octagonal rings, ranging from -0.22 eV to -0.08 eV. However, significantly lower interaction energies were observed within the lattice defects for horizontally aligned CO₂ molecules, about -0.25 eV.

The band structure of pristine BPN exhibits a metallic signature with Dirac cones in the middle of the band. However, a single-atom vacancy disrupts this band profile, eliminating the Dirac cones and resulting in a small bandgap opening of approximately 100 meV. Importantly, BPN does not exhibit precise CO₂ sensing and selectivity by altering its band structure configuration.

Acknowledgements

L.A.R.J acknowledges the financial support from Brazilian Research Council FAP-DF grants 00193–00001247/2021–20, 00193.00001808/2022–71, and 00193–00000857/2021–14, CNPq grants 302236/2018–0 and 350176/2022-1, and FAP-DF-PRONEM grant 00193.00001247/2021 – 20. W.F.G acknowledges the financial support from FAP-DF grant 00193 – 00000811/2021 – 97. This study was financed in part by the Coordenação de Aperfeiçoamento de Pessoal de Nível Superior – Brasil (CAPES) – Finance Code 88887.691997/2022-00. L.A.R.J. gratefully acknowledges the support from ABIN grant 08/2019.

References

- [1] Hui Huang, Wei Feng, and Yu Chen. Two-dimensional biomaterials: material science, biological effect and biomedical engineering applications. *Chemical Society Reviews*, 50(20):11381–11485, 2021.
- [2] Hongjie Tang, Colin M Hessel, Jiangyan Wang, Nailiang Yang, Ranbo Yu, Huijun Zhao, and Dan Wang. Two-dimensional carbon leading to new photoconversion processes. *Chemical Society Reviews*, 43(13):4281–4299, 2014.
- [3] Da Chen, Longhua Tang, and Jinghong Li. Graphene-based materials in electrochemistry. *Chemical Society Reviews*, 39(8):3157–3180, 2010.
- [4] Karim Khan, Ayesha Khan Tareen, Muhammad Aslam, Renheng Wang, Yupeng Zhang, Asif Mahmood, Zhengbiao Ouyang, Han Zhang, and Zhongyi Guo. Recent developments in emerging two-dimensional materials and their applications. *Journal of Materials Chemistry C*, 8(2):387–440, 2020.
- [5] Zhiyu Jia, Yongjun Li, Zicheng Zuo, Huibiao Liu, Changshui Huang, and Yuliang Li. Synthesis and properties of 2d carbon-graphdiyne. *Accounts of chemical research*, 50(10):2470–2478, 2017.
- [6] Ganesh R Bhimanapati, Zhong Lin, Vincent Meunier, Yeonwoong Jung, Judy Cha, Saptarshi Das, Di Xiao, Youngwoo Son, Michael S Strano, Valentino R Cooper, et al. Recent advances in two-dimensional materials beyond graphene. *ACS nano*, 9(12):11509–11539, 2015.
- [7] Andre K Geim and Konstantin S Novoselov. The rise of graphene. *Nature materials*, 6(3):183–191, 2007.
- [8] Huang Wu and Lawrence T Drzal. Graphene nanoplatelet paper as a light-weight composite with excellent electrical and thermal conductivity and good gas barrier properties. *Carbon*, 50(3):1135–1145, 2012.
- [9] Dimitrios G Papageorgiou, Ian A Kinloch, and Robert J Young. Mechanical properties of graphene and graphene-based nanocomposites. *Progress in materials science*, 90:75–127, 2017.
- [10] Hai Yan Nan, Zhen Hua Ni, Jun Wang, Zainab Zafar, Zhi Xiang Shi, and Ying Ying Wang. The thermal stability of graphene in air investigated by raman spectroscopy. *Journal of Raman Spectroscopy*, 44(7):1018–1021, 2013.
- [11] Phaedon Avouris. Graphene: electronic and photonic properties and devices. *Nano letters*, 10(11):4285–4294, 2010.
- [12] Rinaldo Raccichini, Alberto Varzi, Stefano Passerini, and Bruno Scrosati. The role of graphene for electrochemical energy storage. *Nature materials*, 14(3):271–279, 2015.
- [13] He Shen, Liming Zhang, Min Liu, and Zhijun Zhang. Biomedical applications of graphene. *Theranostics*, 2(3):283, 2012.
- [14] Xiangjian Wan, Guankui Long, Lu Huang, and Yongsheng Chen. Graphene—a promising material for organic photovoltaic cells. *Advanced Materials*, 23(45):5342–5358, 2011.
- [15] Frank Schwierz. Graphene transistors. *Nature nanotechnology*, 5(7):487–496, 2010.
- [16] Nathan O Weiss, Hailong Zhou, Lei Liao, Yuan Liu, Shan Jiang, Yu Huang, and Xiangfeng Duan. Graphene: an emerging electronic material.

- Advanced materials*, 24(43):5782–5825, 2012.
- [17] S Yi Zhou, G-H Gweon, AV Fedorov, de First, PN, WA De Heer, D-H Lee, F Guinea, AH Castro Neto, and A Lanzara. Substrate-induced bandgap opening in epitaxial graphene. *Nature materials*, 6(10):770–775, 2007.
- [18] Victor G Desyatkin, William B Martin, Ali E Aliev, Nathaniel E Chapman, Alexandre F Fonseca, Douglas S Galvão, Ericka Roy Miller, Kevin H Stone, Zhong Wang, Dante Zakhidov, et al. Scalable synthesis and characterization of multilayer γ -graphyne, new carbon crystals with a small direct band gap. *Journal of the American Chemical Society*, 144(39):17999–18008, 2022.
- [19] Lingxiang Hou, Xueping Cui, Bo Guan, Shaozhi Wang, Ruian Li, Yunqi Liu, Daoben Zhu, and Jian Zheng. Synthesis of a monolayer fullerene network. *Nature*, 606(7914):507–510, 2022.
- [20] Elena Meirzadeh, Austin M Evans, Mehdi Rezaee, Milena Milich, Connor J Dionne, Thomas P Darlington, Si Tong Bao, Amymarie K Bartholomew, Taketo Handa, Daniel J Rizzo, et al. A few-layer covalent network of fullerenes. *Nature*, 613(7942):71–76, 2023.
- [21] Qitang Fan, Linghao Yan, Matthias W Tripp, Ondřej Krejčí, Stavrina Dimosthenous, Stefan R Kachel, Mengyi Chen, Adam S Foster, Ulrich Koert, Peter Liljeroth, et al. Biphenylene network: A nonbenzenoid carbon allotrope. *Science*, 372(6544):852–856, 2021.
- [22] Fei Pan, Kun Ni, Tao Xu, Huaican Chen, Yusong Wang, Ke Gong, Cai Liu, Xin Li, Miao-Ling Lin, Shengyuan Li, et al. Long-range ordered porous carbons produced from c60. *Nature*, pages 1–7, 2023.
- [23] Chee-Tat Toh, Hongji Zhang, Junhao Lin, Alexander S Mayorov, Yun-Peng Wang, Carlo M Orofeo, Darim Badur Ferry, Henrik Andersen, Nurbek Kakenov, Zenglong Guo, et al. Synthesis and properties of free-standing monolayer amorphous carbon. *Nature*, 577(7789):199–203, 2020.
- [24] Yiming Hu, Chenyu Wu, Qingyan Pan, Yinghua Jin, Rui Lyu, Vikina Martinez, Shaofeng Huang, Jingyi Wu, Lacey J Wayment, Noel A Clark, et al. Synthesis of γ -graphyne using dynamic covalent chemistry. *Nature Synthesis*, 1(6):449–454, 2022.
- [25] Guogang Liu, Tong Chen, Xiaohui Li, Zhonghui Xu, and Xianbo Xiao. Electronic transport in biphenylene network monolayer: Proposals for 2d multifunctional carbon-based nanodevices. *Applied Surface Science*, 599:153993, 2022.
- [26] Hsin-Tsung Chen and Dinesh Kumar Dhanthala Chittibabu. A new carbon allotrope: Biphenylene as promising anode materials for li-ion and lio2 batteries. *Solid State Ionics*, 395:116214, 2023.
- [27] David Ferguson, Debra J Searles, and Marlies Hankel. Biphenylene and phagraphene as lithium ion battery anode materials. *ACS applied materials & interfaces*, 9(24):20577–20584, 2017.
- [28] Yuewen Mu and Si-Dian Li. Superconducting and transport properties of biphenylene network monolayer with alkaline metal adatoms. *Applied Surface Science*, page 157255, 2023.
- [29] Razieh Esfandiarpour, Fatemeh Zamanian, Farideh Badalkhani-Khamseh, and Mohammad Reza Hosseini. Carbon dioxide sensor device based on biphenylene nanotube: A density functional theory study. *Computational and Theoretical Chemistry*, 1218:113939, 2022.
- [30] Wan-Sheng Su and Chen-Hao Yeh. Theoretical investigation of methane oxidation reaction over a novel metal-free catalyst biphenylene network. *Diamond and Related Materials*, 124:108897, 2022.
- [31] Ashish Kumar Mishra and Sundara Ramaprabhu. Carbon dioxide adsorption in graphene sheets. *AIP Advances*, 1(3):032152, 2011.
- [32] Pepa Cabrera-Sanfeliix. Adsorption and reactivity of co2 on defective graphene sheets. *The Journal of Physical Chemistry A*, 113(2):493–498, 2009.
- [33] Kaori Takeuchi, Susumu Yamamoto, Yuji Hamamoto, Yuichiro Shiozawa, Keiichiro Tashima, Hirokazu Fukidome, Takanori Koitaya, Kozo Mukai, Shinya Yoshimoto, Maki Suemitsu, et al. Adsorption of co2 on graphene: a combined tpd, xps, and vdW-df study. *The Journal of Physical Chemistry C*, 121(5):2807–2814, 2017.
- [34] B. Delley. An all-electron numerical method for solving the local density functional for polyatomic molecules. *The Journal of Chemical*

- Physics*, 92(1):508–517, 1990.
- [35] B. Delley. From molecules to solids with the dmol3 approach. *The Journal of Chemical Physics*, 113(18):7756–7764, 2000.
- [36] Dassault Systèmes. Biovia materials studio. *San Diego*, 2017.
- [37] Stefan Grimme. Semiempirical gga-type density functional constructed with a long-range dispersion correction. *Journal of computational chemistry*, 27(15):1787–1799, 2006.
- [38] Georg Kresse and Daniel Joubert. From ultrasoft pseudopotentials to the projector augmented-wave method. *Physical review b*, 59(3):1758, 1999.
- [39] John P Perdew, Kieron Burke, and Matthias Ernzerhof. Generalized gradient approximation made simple. *Physical review letters*, 77(18):3865, 1996.
- [40] B Delley. Hardness conserving semilocal pseudopotentials. *Physical Review B*, 66(15):155125, 2002.
- [41] Hendrik J Monkhorst and James D Pack. Special points for brillouin-zone integrations. *Physical review B*, 13(12):5188, 1976.
- [42] Kleuton A Lopes Lima, Marcelo L Pereira Júnior, Fábio F Monteiro, Luiz F Roncaratti, and Luiz A Ribeiro Júnior. O₂ adsorption on defective penta-graphene lattices: A dft study. *Chemical Physics Letters*, 763:138229, 2021.
- [43] Igo T Lima, Ricardo Gargano, Silvette Guerini, and Edson NC Paura. A theoretical study of adsorbed non-metallic atoms on magnesium chloride monolayers. *New Journal of Chemistry*, 43(20):7778–7783, 2019.
- [44] Edson NC Paura, Wiliam F da Cunha, João Batista Lopes Martins, Geraldo Magela e Silva, Luiz F Roncaratti, and Ricardo Gargano. Carbon dioxide adsorption on doped boron nitride nanotubes. *Rsc Advances*, 4(54):28249–28258, 2014.
- [45] Michael Rivera Mananghaya. Adsorption of co and desorption of co₂ interacting with pt (111) surface: a combined density functional theory and kinetic monte carlo simulation. *Adsorption*, 26(3):461–469, 2020.
- [46] Kleuton Antunes Lopes Lima, Wiliam Ferreira da Cunha, Fábio Ferreira Monteiro, Bernhard Georg Enders, Marcelo Lopes Pereira Jr, and Luiz Antonio Ribeiro Jr. Adsorption of carbon dioxide and ammonia in transition metal-doped boron nitride nanotubes. *Journal of Molecular Modeling*, 25:1–7, 2019.
- [47] A Bafekry, M Faraji, MM Fadelallah, HR Jappor, S Karbasizadeh, M Ghergherehchi, and D Gogova. Biphenylene monolayer as a two-dimensional nonbenzenoid carbon allotrope: a first-principles study. *Journal of Physics: Condensed Matter*, 34(1):015001, 2021.
- [48] Bohayra Mortazavi and Alexander V Shapeev. Anisotropic mechanical response, high negative thermal expansion, and outstanding dynamical stability of biphenylene monolayer revealed by machine-learning interatomic potentials. *FlatChem*, 32:100347, 2022.
- [49] Obaidur Rahaman, Bohayra Mortazavi, Arezoo Dianat, Gianaurelio Cuniberti, and Timon Rabczuk. Metamorphosis in carbon network: From penta-graphene to biphenylene under uniaxial tension. *FlatChem*, 1:65–73, 2017.
- [50] Biplab Sanyal, Olle Eriksson, Ulf Jansson, and Helena Grennberg. Molecular adsorption in graphene with divacancy defects. *Physical Review B*, 79(11):113409, 2009.
- [51] Kriengkri Timsorn and Chatchawal Wongchoosuk. Adsorption of NO₂, HCN, HCHO and CO on pristine and amine functionalized boron nitride nanotubes by self-consistent charge density functional tight-binding method. *Materials Research Express*, 7(5):055005, may 2020.